Radical involved reaction and weak magnetic effect between alumina refractory and high alumina slags

A Huang[1], S. H Li[2], H. Z Gu[3]

1.Professor, the State Key Laboratory of Refractories and Metallurgy, Wuhan China 430081. Email: huangao@wust.edu.cn
2.Doctor, the State Key Laboratory of Refractories and Metallurgy, Wuhan China 430081. Email: lishenghao@wust.edu.cn
3.Professor, the State Key Laboratory of Refractories and Metallurgy, Wuhan China 430081. Email: guhuazhi@wust.edu.cn

Keywords: Alumina refractory; CaO-Al_2O_3-SiO_2 slag; radiation spectrum; free radical reaction; weak magnetic effect

ABSTRACT

High aluminum steel is a promising advanced steel known for its exception properties and holds significant economic and strategic importance. However, the $CaO-Al_2O_3-SiO_2$ based slag with high alumina content reacts vigorously with alumina refractories during the smelting process at high temperature, seriously affecting the safe and efficient production of furnaces and resulting in the formation of Al_2O_3-MgO non-metallic inclusions within the molten steel. This is a bottleneck problem for high-quality steel refining, and the key reaction path during the corrosion remains unclear.

The dissolution reaction mechanism of alumina refractories in high alumina $CaO-Al_2O_3-SiO_2$ slags under a weak static magnetic field was investigated in this work, using high temperature laser confocal microscopy and in-situ radiation spectroscopy techniques. The results indicate that the interaction between the high alumina slags and the alumina refractories is governed by free radical reactions. The dissolution of alumina forms AlO and AlO_2 radicals. The reaction rate increases with the C/S ratio of the slag due to its low polymerization. The reaction between non-bridging oxygen and AlO_2 free radicals accelerates the generation of AlO and $O_2^{\cdot-}$ radicals. The reaction layer composed of calcium aluminate is formed through the recombination of AlO, $Ca^{\cdot+}$, and $O_2^{\cdot-}$ radicals. The weak static magnetic field induces the Zeeman splitting of free radical pairs and intersystem crossing occurs, promoting the formation of triplet free radical pairs through the hyper-fine coupling effect. The reaction can be significantly inhibited as the triplet free radical pair does not meet Pauli's incompatibility principle. This discovery perfects the structure theory of molten slags with radicals and provides supplement to the design of the highly slag-resistant refractories, and provides the theoretical basis for the development of external field protection technologies for high-quality steel refining.

INTRODUCTION

High aluminum steel, distinguished by its remarkable strength, plasticity, high strain hardening, and energy absorption capacity, shows broad prospects in applications in national defense, military industries, and transportation sectors (Zuazo et al., 2014; Zhang et al., 2015). The use of $CaO-Al_2O_3-SiO_2$ and $CaO-Al_2O_3$ slags are widely used for high aluminum steel refining (He et al., 2020; Zhang et al., 2002; Zhao et al., 2021; Tang et al., 2017; Wang et al., 2012; Wang et al., 2019), and the high alumina steel can cause the formation of high alumina content slag, which can cause continuous and periodic corrosion patterns at the reaction interface of the slag and the corundum refractory, resulting in rapid dissolution and damage to the refractory (Zou et al., 2020a). The periodicity of corrosion patterns is unrelated to the spatiotemporal evolution, but its geometric parameters was highly correlated with the C/S ratio and the dissolution rate of aluminum (Li et al., 2021). Free radicals were discovered in the $CaO-Al_2O_3-SiO_2$ based slag, and the recombination of AlO_4 and SiO_4 tetrahedra in the slag of higher C/S ratio is one of the causes for the formation of radicals. $O_2^{\cdot-}$ and $Ca^{\cdot+}$ radicals involved in the interface reaction between the corundum refractory and the slag, the Turing pattern corrosion at the interface of alumina ceramic is caused by an increase in $O_2^{\cdot-}$ radical content in the slag (Li et al., 2023; Peng et al., 2023a, 2023b).

This not only affects the safe and efficient operation of furnaces (Dong et al., 2021; Jiang et al., 2022), but also leads to the formation of non-metallic inclusions in the steel, which is one of the key bottlenecks restricting the development of high-quality steel smelting (Wang et al., 2023; Liu et al., 2023; Zhou et al., 2015; Tsuda et al., 1992).

With the development of modern metallurgical technology, electric field and magnetic field have been widely used in metallurgical processes such as electroslag remelting, electromagnetic induction melting, electromagnetic stirring, and electromagnetic continuous casting. The physical parameters of slag and the service life of refractories can be affected by external high-intensity electric and magnetic fields. The alternating magnetic field promotes the interface reaction between slag and refractories, accelerating the corrosion and penetration of slag on the refractories (Aneziris et al., 2008; Ren et al., 2019, 2020), whereas the static magnetic field has the effect of enhancing the corrosion degree of slag on refractory (Huang et al., 2018).

An 8.5 mT static magnetic field can induce an “electromagnetic damping effect” on the slag, leading to a reduction in wettability between the slag and the refractory (Zou et al., 2020b). However, the physical effects of the magnetic field, such as electromagnetic damping and polarization of the reactive group, can only be fully utilized when the magnetic flux density and frequency are high enough to improve the slag resistance of the refractory (Bian, 2018). Different from the electric field, high intensity magnetic field or alternating magnetic field, it was also found that the weak static magnetic field with a millitesla magnetic flux density has the potential to improve the slag resistance of refractories. The weak static magnetic field of 5 to 10 Gs can influence the chemical reactions between slag and alumina-based refractories, and delaying the occurrence of interface Turing pattern corrosion (Li et al., 2022, 2023). Weak static magnetic field has the potential to inhibit the chemical reactions between slag and alumina refractories, offering possibilities for enhancing the slag resistance of the refractory.

However, the interaction between alumina refractories and high alumina slag is rather complex. The lack of information during corrosion at high temperatures limits the exploration of reaction mechanisms (Zhang et al., 2021; Ponomar et al., 2022). In this work, the dissolution reaction mechanism of alumina refractory in high alumina CaO-Al_2O_3-SiO_2 slags under a weak static magnetic field was clarified, and the key reaction path and magnetic field inhibition mechanism were revealed based on high temperature laser confocal microscopy and in-situ radiation spectroscopy techniques.

EXPERIMENTAL

Al_2O_3 powder (analytical purity, Al_2O_3≥99 wt%, Shanghai Macklin Biochemical Co., Ltd), CaO powder (analytical purity, CaO≥98 wt%, Shanghai Macklin Biochemical Co., Ltd), and SiO_2 powder (analytical purity, SiO_2≥98wt%, Sinopharm Chemical Reagent Co., Ltd) were weighed according to the mass ratios presented in Table 1. The powder were mixed via ball milling at a speed of 60 r/min for 30 minutes. Afterward, the mixed power were pre-melted in a high-frequency induction furnace (Supersonic Frequency Induction Heating Equipment, Hubei Changjiang Precision Manufacturing Technology Co., Ltd). The molten slag was then poured onto a copper plate floating above

circulating water to prevent the molten slag from segregating and crystallizing. Subsequently, the glassy molten was ground in an agate mortar. The alumina balls (Al_2O_3: 95wt%, SiO_2: 4.5wt%, CaO: 0.5wt%, ρ=3.8g/cm^3) with a diameter of 1.20 ± 0.05 mm and a mass of 3.45 ± 0.05 mg were selected as alumina refractories.

TABLE 1 Composition of the pre-melted powders (wt %)

No.	CaO	Al_2O_3	SiO_2	C/S ratio
S1	52.00	35.00	13.00	4
S2	54.17	35.00	10.82	5
S3	55.71	35.00	9.29	6

0.2 g of pre-melted slag was compresses into a platinum crucible measured 8 mm in diameter and 4 mm in height. The crucible was placed on the high temperature laser confocal microscope (HT-CSLM, VL2000DX-SVF18SP, Mikura Seisakusho Co., Ltd., Japan) and heated to 1600 °C in an argon atmosphere (the heating ratio referred to Li et al., 2022). After soaking at 1600 °C for 180 s, the alumina ball was fed into the slag by using the High-Temperature Anti-oxidation Feeding System (GC-500901, Mikura Seisakusho Co., Ltd.). A pair of magnetic as shown in Figure 1 applied a static magnetic field throughout the experiment and it could be adjusted by changing the number of magnets. The flux density of static magnetic in the reaction region was calibrated using a Tesla meter (Changsha Tianheng Measurement and Control Technology Co., Ltd.). The magnetic flux density for each sample as shown in Table2.

The in-situ radiation spectroscopic system is composed of a spectrograph (Avenir GmbH, Germany) and a filter group. The radiation passing through the filter group, and the transmitted through a cosine corrector (Avenir GmbH, Germany) and finally analyzed by the spectrograph, as shown in Figure 1. The radiation spectrum and the morphology of alumina refractory in dissolution process were recorded by the device.

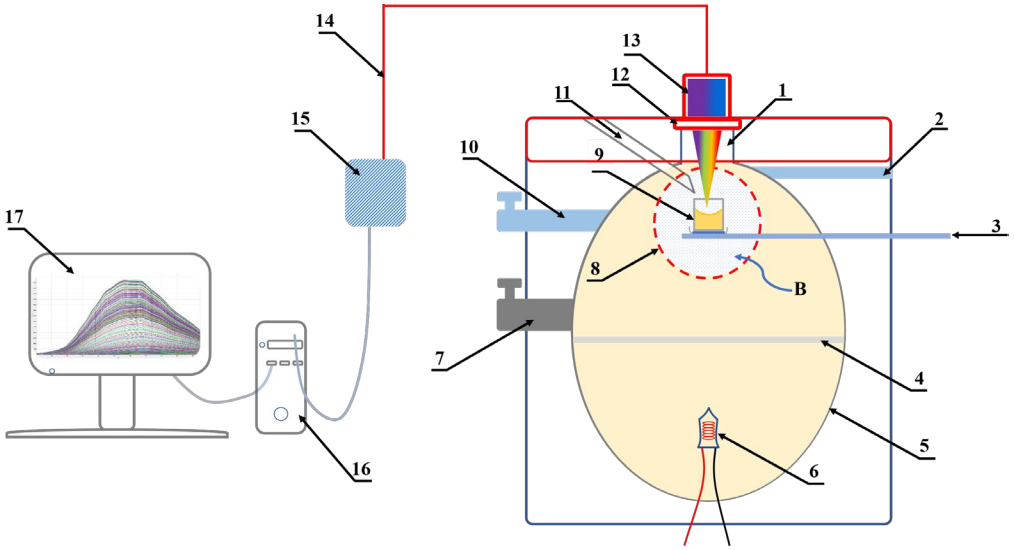

1-Quartz window; 2-Gas outlet valve; 3-Thermocouple with platinum stent; 4-Quartz spacer; 5-Furnace chamber; 6-Halogen lamp
7-Vacuum valve; 8-NdFeB magnet; 9-Pt crucible; 10-Intake valve; 11-oxidation protection feeder; 12-Filter group; 13-Cosine corrector
14- Fibre-optical; 15-Spectrograph; 16-Computing system; 17-Signal output system

FIG 1 Schematic diagram of the device

TABLE 2 Magnetic flux density produced in the experimental area

No.	Magnetic flux density/ Gs	
S1	0	15
S2	0	10
S3	0	10

The quenched samples were longitudinally cut, and polished and gold-plated using vacuum ion sputtering, the microstructure and composition at the interface between slag and alumina balls were analysed by scanning electron microscope (SEM, JSM-6610, JEOL, Tokyo, Japan) and energy dispersive X-Ray spectroscopy (EDX, QUANTAX, Bruker, Berlin, Germany). The synthetic slag was ground into micropowder (0.074 mm), and the superoxide radicals were analyesd using electron paramagnetic resonance spectrometer (EPR, A300, Bruker, Saarbrücken, Germany) with DMPO capture agent in a non-light environment.

The average dissolution rate of alumina balls is determined by (Huo et al., 2022):

$$\bar{v}=\frac{\Delta W}{\bar{A}\cdot t} \quad (1)$$

$$\bar{A}=\pi D^2 \quad (2)$$

Where ΔW is the mass change of the alumina ball during dissolution, g; $\bar{A}$ is the average superficial area of the alumina ball, cm^2; D is the diameter of the alumina ball, cm; and t is the dissolution time, s.

RESULTS AND DISSCUSSION

Weak magnetic field effect on the dissolution of alumina balls

The rapid dissolution of alumina balls in the high alumina content slag refer to Figure 2), and the dissolution rate increased with the increasing C/S ratio of the slag as shown in Figure 3. However, the dissolution can be significantly inhibited by the external weak static magnetic field, and the dissolution rates of alumina balls in slag S1~S3 experienced a decrease of approximately 20.3%, 27.5%, and 35.0%, respectively.

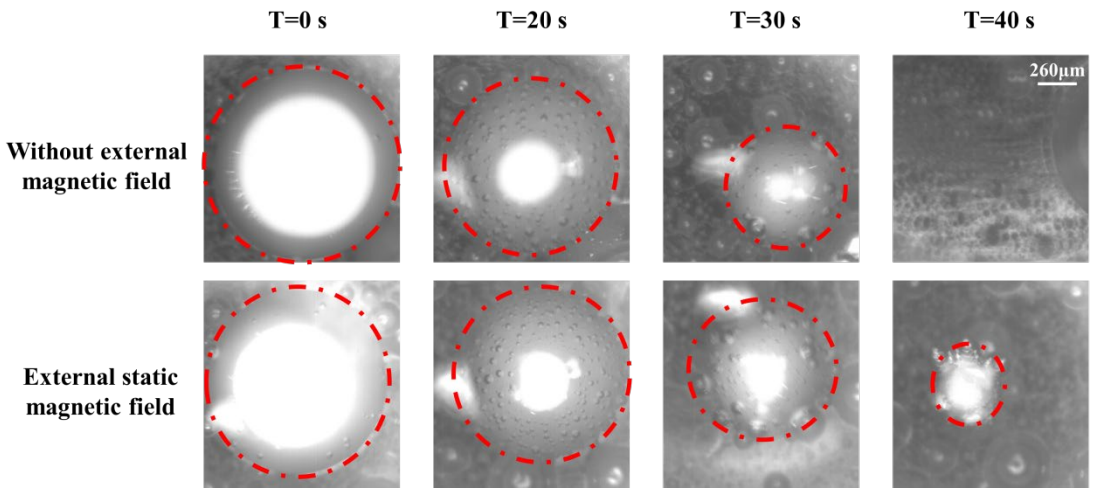

FIG 2 The recorded picture of the dissolution process of alumina balls in slag at 1600 °C

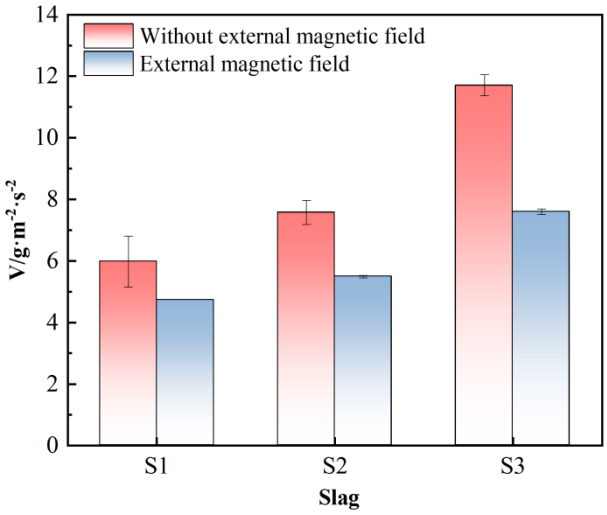

FIG 3 Dissolution rate of alumina balls in slags

As an illustration, S3 slag was utilized to investigate, the microstructure of the reaction interface between the alumina balls and the slags during the dissolution was analysed, as shown in Figure 4. A reaction layer composed of calcium aluminate with a thickness of 76.32 μm was observed at the reaction interface as shown in Figure 4 and Table 3, when an external weak static magnetic field was applied the thickness of the layer was reduced reduced to 41.25 μm.

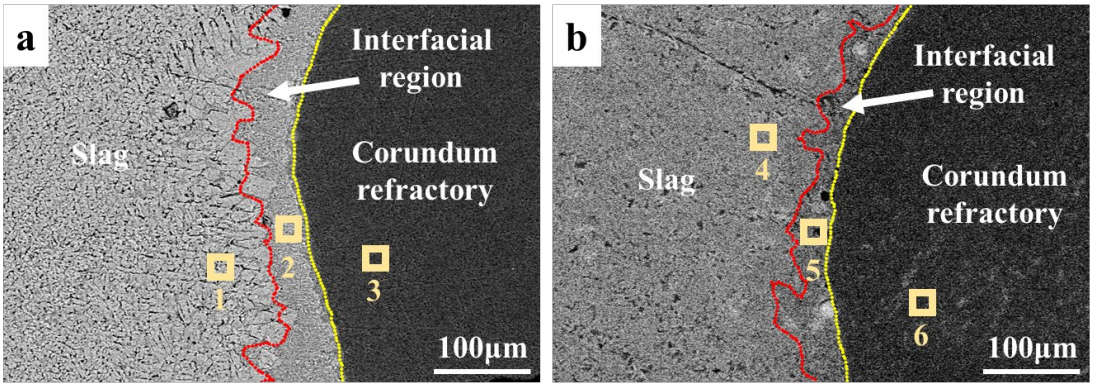

FIG 4 Microstructure of the reaction interface between the alumina ball and melts at 1600 °C in 20 s, a: without static magnetic field, b: with weak static magnetic field

TABLE 3 EDS analysis results (at%)

Area	Ca	Al	Si	O
Area 1	-	45.76	-	54.24
Area 2	23.35	18.11	2.43	56.12
Area 3	25.87	16.54	2.19	55.40
Area 4	-	45.50	-	54.50
Area 5	24.07	19.29	2.62	54.02
Area 6	28.07	13.38	1.73	56.82

Radical reaction mechanism in the dissolution of alumina balls

The concentration of superoxide radicals in the slags increased with the increasing C/S ratio, as shown by the stronger signals in Figure 5a. Additionally, the concentration of superoxide radicals in the slags gradually increased with the dissolution of alumina balls, as shown in Figure 5b.

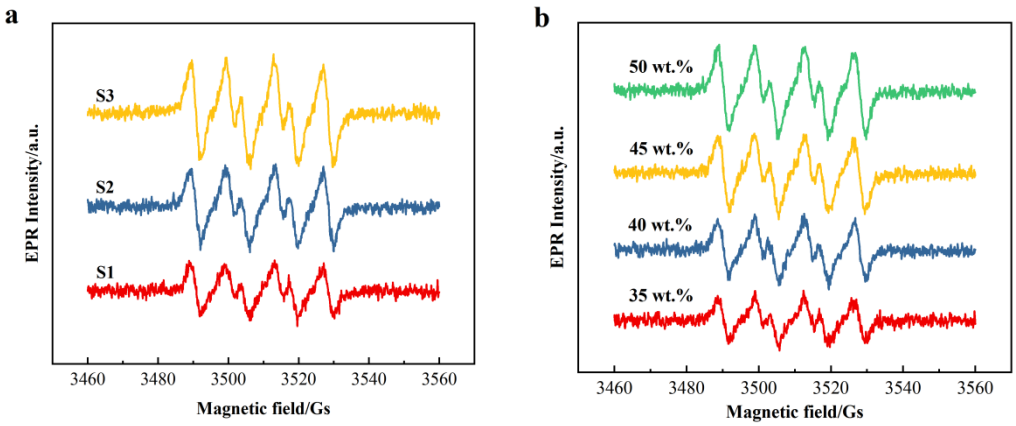

FIG 5 a: EPR spectra of S1~S3 slag; b: EPR spectra of S3 slag with the increase of alumina concentration

Comparing the radiation spectra before and during the reaction at 1600 °C, a signal at 484.21 nm was detected (as shown in Figure 6a), indicating the formation of AlO radical (Varenne et al., 2000; Starik A et al, 2014). The signal intensity gradually increased with the increase in the C/S ratio, indicating a higher formation of AlO radical. The application of an external static magnetic field inhibited the generation of AlO radical as shown in Figure 6b.

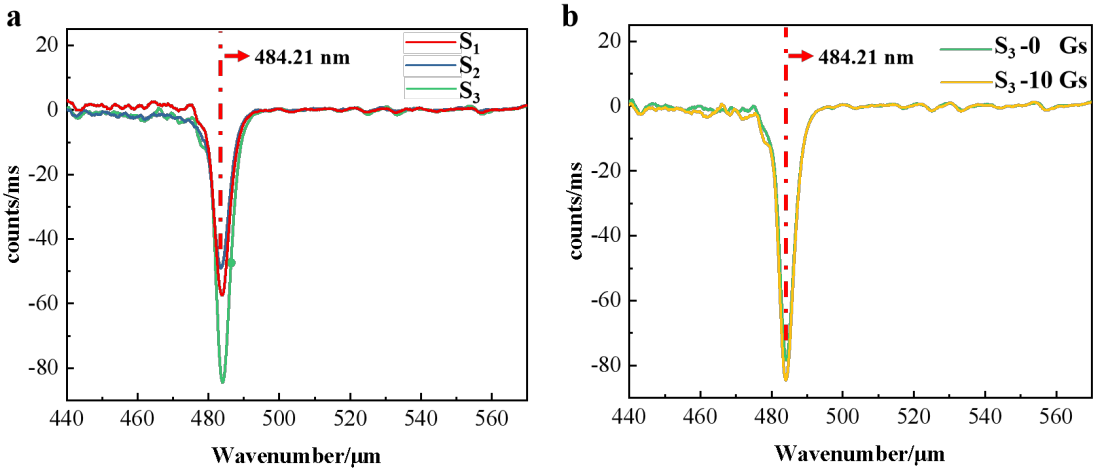

FIG 6 In situ radiation spectrum during the alumina dissolution, a: in S1~S3 slags, b: in S3 slag with and without external static magnetic field

The reaction path between the alumina refractory and the slag is as Eqn. (3) and Eqn. (4). The AlO and AlO_2 radicals can be generated by the homolysis of Al_2O_3 in molten slag, the non-bridging oxygen can be attacked by AlO_2 radicals, which accelerates the dissolution of alumina refractory and generates $O_2^{\cdot-}$.

$$Al_2O_3 \rightarrow AlO + AlO_2 \quad (3)$$

$$AlO_2 + O^- \rightarrow AlO + O_2^{\cdot-} \quad (4)$$

Non-bridging oxygen (O^-) in slag plays a crucial role. In slags characterized by a higher (C/S) ratio, a greater concentration of non-bridging oxygen, as indicated by Li et al. (2023), facilitates reaction (4) and resulting in the rapid dissolution of alumina refractory.

According to our previous investigations (Li et al., 2021, 2022, 2023; Peng et al., 2023a, 2023b) have indicated that $O_2^{\cdot-}$ and $Ca^{\cdot+}$ are formed spontaneously through the uniform decomposition of CaO_2 in the CaO-Al_2O_3-SiO_2 slag. The reaction layer composed of calcium aluminate can be formed through the recombination of AlO, $Ca^{\cdot+}$, and $O_2^{\cdot-}$ radicals at the reaction interface as shown in equation (5) and Figure 7.

$$2AlO + Ca^{\cdot+} + O_2^{\cdot-} \rightarrow CaAl_2O_4 \quad (5)$$

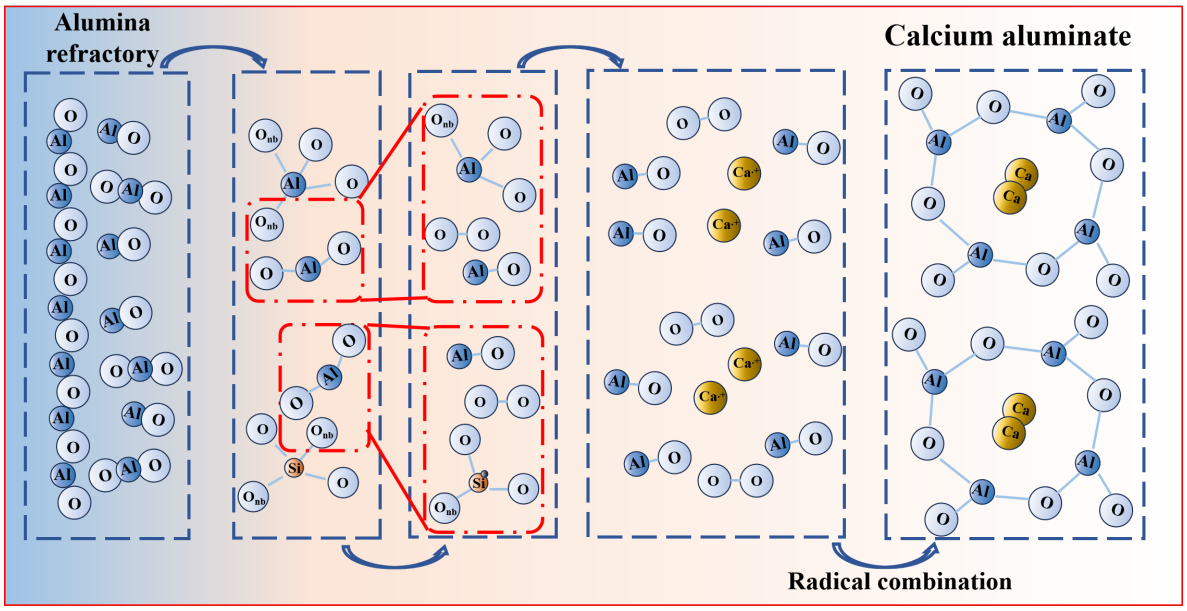

FIG 7 Possible radical reaction mechanism at the interface between the alumina refractory and the molten slags

The energy formula for singlet and triplet state free radical pairs with the external static magnetic field is given by (Zimmt et al., 1985):

$$E(S) = \langle S, \chi_N | H_{ex} + H_{mag} | S, \chi_N \rangle = J \tag{6}$$

$$E(T_n) = \langle T_n, \chi_N | H_{ex} + H_{mag} | T_n, \chi_N \rangle = -J + ng\mu_B B + \frac{n}{2}(\sum_i^j a_i m_i + \sum_k^l a_k m_k) \tag{7}$$

where a_i is the hyperfine coupling constant of the i atom and m_i is the spin quantum number of the i nucleus.

According to equations (6) and (7), it is clear that the Zeeman splitting (represented by $g\mu_B \cdot B$) of free radical pairs induced by the static magnetic field is the main factor affecting the energy of free radicals in the singlet and triplet states. When an external magnetic field with the appropriate flux density is applied and the Zeeman splitting energy matches the energy difference of the free radical pairs, the intersystem crossing occurs under the hyperfine coupling effect as shown in Figure 8. The transformation of free radical pairs from singlet to triplet states (Sarpoolaky et al., 2003; Hayashi H, 2004) results in a reduction of the bonding probability of free radicals, thereby inhibiting chemical reactions of (4) and (5), and decreasing the interfacial reaction and the dissolution rate of alumina balls in the slags.

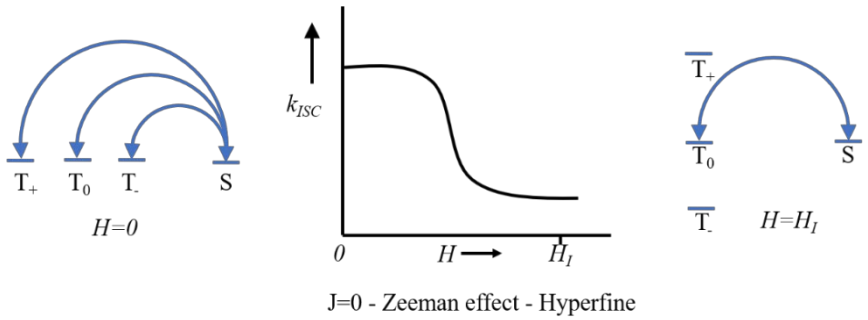

FIG 8 Effect of magnetic field on the radical intersystem crossing (Hayashi H, 2004)

CONCLUSIONS

The dissolution mechanization of the alumina refractory in high alumina content slag was clarified based on high temperature laser confocal microscopy combined with in-situ radiation spectroscopy techniques. The radical reaction path and the effect of weak static magnetic field during the dissolution of alumina refractory was revealed. The main conclusions are as follows.

(1) Alumina refractory involved in the intense interfacial radical reaction with high alumina content slag, resulting in the rapid dissolution of refractory and the formation of a calcium aluminate reaction layer on the refractory/slag interface. Free radical splays a crucial role in the process, however when a static magnetic field is applied, the reaction rate decreases significantly and the thickness of the calcium aluminate reaction layer. Taking S3 slag as an example, the dissolution rate of the alumina ball decreased by 35.0%, and the thickness of the interface reaction layer decreased by 46.0% with external the static magnetic field.

(2) The reaction path between alumina refractory and the slag was revealed. Free radicals including AlO, AlO_2, and $O_2^{\cdot -}$ were generated during the dissolution of alumina refractory at 1600 °C. The reaction layer composed of calcium aluminate is formed through the recombination of AlO, $Ca^{\cdot +}$, and $O_2^{\cdot -}$ radicals at the reaction interface$^{\cdot -}$. For the slag with a higher C/S ratio, the non-bridging oxygen was attacked by AlO_2 radicals, thereby accelerating the dissolution rate of alumina refractory.

(3) The weak static magnetic field induces the Zeeman splitting of free radical pairs and enhances the hyperfine coupling, resulting in intersystem crossing from singlet to triplet states. The radical reactions are inhibited as the triplet free radical pair does not meet Pauli's incompatibility principle. This reduces the interfacial reaction rate between alumina refractories and slags. This work perfects the structure theory of molten slags with radicals and supports the development of external field protection techniques for carbon-free/low-carbon refractories, which is significant for the safe and efficient production of high-quality steel.

ACKNOWLEDGEMENTS

This work was financially supported by the National Natural Science Foundation of China (52272022), Key Program of Natural Science Foundation of Hubei Province (2021CFA071)

REFERENCES

Aneziris C G, Schroeder C, Emmel M, et al, 2013. In situ observation of collision between exogenous and endogenous inclusions on steel melts for active steel filtration, Metallurgical and Materials Transactions B, 44: 954-968.

Bian Y, Ding W, Hu L, et al, 2018. Acceleration of Kirkendall effect processes in silicon nanospheres using magnetic fields. CrystEngComm, 20(6): 710-715.

Dong, J, 2021. Fabrication of Calcium Hexaaluminate Based Castable and Its Properties of Resistance to High-alumina CaO-Al_2O_3-SiO_2 slags, Wuhan University of Science and Technology (Wuhan).

Hayashi H, 2004. Introduction to dynamic spin chemistry: magnetic field effects on chemical and biochemical reactions. World Scientific.

He, S, Chen, Y, Pan, W, et al, 2020. Study on composition control for melting and flowing properties of CaO-Al_2O_3 based mold fluxes with low reactivity. Journal of Iron and Steel Research, 32(9):771-778.

Huo, Y, Gu, H, Huang, A, et al, 2022. Characterization and mechanism of dissolution behavior of Al_2O_3/MgO oxides in molten slags, Journal of Iron and Steel Research International, 29(11):1711-1722.

Huang A, Lian P, Fu L, et al, 2018. Towards retardation of slag corrosion on the lightweight alumina refractory with static magnetic field facing green metallurgy. Journal of Mining and Metallurgy, Section B: Metallurgy, 54(2): 143-143.

Jiang, X, Huang, A, Gu, H, et al, 2022. Effect of Al_2O_3 content in CaO-Al_2O_3-SiO_2 slag on corrosion resistance of alumina magnesia castable, Journal of Iron and Steel Research, 34(9):991-998.

Li, S, Huang, A, Jiang, T, et al, 2023. Revealing of rich living radicals in oxide melts via weak magnetic effect on alumina dissolution reaction, Journal of Molecular Liquids, 375:121391.

Li, S, Huang, A, Gu, H, et al, 2022. Corrosion resistance and anti-reaction mechanism of Al_2O_3-based refractory ceramic under weak static magnetic field, Journal of the American Ceramic Society, 2022, 105(4):2869-2877.

Li, S, Huang, A, Gu, H, et al, 2021. Visual measurement and characterisation of quasi-volcanic corrosion at alumina ceramic-oxides melt-air interface, Journal of the European Ceramic Society, 41(16):400-410.

Liu, D, Xue, Z, Song, S, 2023. Effect of cooling rate on non-metallic inclusion formation and precipitation and micro-segregation of Mn and Al in Fe-23Mn-10Al-0.7 C steel, Journal of Materials Research and Technology, 24:4967-4979.

Peng, Y, Li, S, Huang, A, et al, 2023a. Effect of slag basicity on turing pattern corrosion of alumina refractory ceramics in the presence of free radicals, Journal of the American Ceramic Society, 106(10):6211-6220.

Peng, Y, Huang, A, Li, S, et al, 2023b. Radical reaction-induced Turing pattern corrosion of alumina refractory ceramics with CaO-Al_2O_3-SiO_2-MgO slags, Journal of the European Ceramic Society, 43(1):166-172.

Ponomar, V, Adesanya, E, Ohenoja, K, et al, 2022. High-temperature performance of slag-based Fe-rich alkali-activated materials, Cement and Concrete Research, 161:106960.

Ren X, Ma B, Li S, et al, 2019. Slag corrosion characteristics of MgO-based refractories under vacuum electromagnetic field, Journal of the Australian Ceramic Society, 55: 913-920.

Ren X, Ma B, Li S, et al, 2021. Comparison study of slag corrosion resistance of MgO-$MgAl_2O_4$, MgO-CaO and MgO-C refractories under electromagnetic field. Journal of Iron and Steel Research International, 28: 38-45.

Sarpoolaky, H, Zhang, S, Lee, W, 2003. Corrosion of high alumina and near stoichiometric spinels in iron containing silicate slags, Journal of European Ceramic Society, 23(2):293-300.

Starik A M, Kuleshov P S, Sharipov A S, et al, 2014. Kinetics of ignition and combustion in the Al–CH_4–O_2 system. Energy & fuels, 28(10): 6579-6588.

Tang, H, Wu, G, Wang, Y, et al, 2017. Comparative evaluation investigation of slag corrosion on Al_2O_3 and MgO-Al_2O_3 refractories via experiments and thermodynamic simulations, Ceramics International, 43(18):16502-16511. Ceramics International, 45(16):20664-20673.

Tsuda, M, Yamaguchi, H, Kaneko, K, et al, 1992. Production of ultra super purity ferritic stainless steel by the powder top blowing method under reduced pressure(VOD-PB), Electric Furnace Conference Proceedings, 50:259-262.

Varenne, O, Fournier, P G, Fournier, J, et al, 2000. Internal population distribution of the B state of AlO formed by fast ion beam bombardment or laser ablation of an Al_2O_3(Al) surface, Nuclear Instruments and Methods in Physics Research Section B: Beam Interactions with Materials and Atoms, 171(3):259-276.

Wang, D, Li, X, Wang, H, et al, 2012. Dissolution rate and mechanism of solid MgO particles in synthetic ladle slags, Journal of Non-Crystalline Solids, 358(9):1196-1201.

Wang, W, Xue, L, Zhang, T, et al, 2019. Thermodynamic corrosion behavior of Al_2O_3, ZrO_2 and MgO refractories in contact with high basicity refining slag, Ceramics International, 45(16):20664-20673.

Wang, J, Song, S, Xue, Z, 2023. Transient evolution of non-metallic inclusions in molten high aluminum and high manganese steel contacting with slag and crucible: experimental investigation and FactSage macros modeling, Journal of Materials Research and Technology, 25:2841-2853.

Zhang, M, Chen, W, Cheng, Z, et al, 2015. Influence of Physical Property of Silicon Steel Slag with High Alumina on Ladle Slag Buildup, Bulletin of the Chinese Ceramic Society, 34(4):1160-1164.

Zhang, D, Wang, H, 2002. Corrosion behavior of refining slags with different basicities to corundum-spinel castable, Naihuo Cailiao, 36(4):215-217.

Zhao, X, Zhang, R, Jia, J, et al, 2021. Effect of basicity on the microstructure of molten slag of CaO-SiO_2-Al_2O_3 system, Journal of Materials and Metallurgy, 20(3):179-184.

Zhou, M, Yang, S, Jiang T, et al, 2015. Influence of MgO in form of magnesite on properties and mineralogy of high chromium, vanadium, titanium magnetite sinters, Ironmaking & Steelmaking, 42(4):320-320.

Zhang, J, Wang, C, Jiao, K, et al, 2021. Effect of BaO and MnO on high-temperature properties and structure of blast furnace slag, Journal of Non-Crystalline Solids, 571:121066.

Zimmt, M B, Doubleday, J C, Turro, N J, 1985. Magnetic field effect on the intersystem crossing rate constants of biradicals measured by nanosecond transient UV absorption, Journal of the American Chemical Society, 107(23):6726-6727.

Zou, Y, Huang, A, Gu, H, 2020a. Novel phenomenon of quasi-volcanic corrosion on the alumina refractory-slag-air interface, Journal of the American Ceramic Society, 103(11):6639-6649.

Zou Y, Huang A, Wang R, et al, 2020b. Slag corrosion-resistance mechanism of lightweight magnesia-based refractories under a static magnetic field. Corrosion Science, 167: 108517.

Zuazo, I, Hallstedt, B, Lindahl, B, et al, 2014. Low-density steels: complex metallurgy for automotive applications, JOM, 66(9):1747-1758.